Epoxy-based nanocomposites for electrical energy storage. II: Nanocomposites with nanofillers of reactive montmorillonite covalently-bonded with barium titanate

G. Polizos,[1,2] V. Tomer,[2,3] E. Manias,[1,a)] and C. A. Randall[2,a)]
[1]*Polymer Nanostructures Laboratory, Center for the Study of Polymeric Systems (CSPS) and Department of Materials Science and Engineering, The Pennsylvania State University, University Park, Pennsylvania 16802, USA*
[2]*Center of Dielectric Studies (CDS), Materials Research Laboratory and Department of Materials Science and Engineering, The Pennsylvania State University, University Park, Pennsylvania 16802, USA*
[3]*The Dow Chemical Co., Corporate R&D, Midland, Michigan 48674, USA*

(Received 16 February 2010; accepted 15 July 2010; published online 15 October 2010)

Barium titanate (BT) and montmorillonite (MMT) nanoparticles were covalently-bonded by organically modifying the particle surfaces and chemically reacting them in solution. These integrated two-material hybrid inorganic nanofillers were subsequently dispersed in epoxy resin and nanocomposites were obtained at several weight fractions. The inorganic component consisted of well dispersed BT spherical nanoparticles that are surrounded by attached layered MMT nanoplatelets, with the latter having the ability to react with the epoxy matrix. The thermodynamic properties of the glass transition process, the macroscopic mechanical properties of the nanocomposites, and the dynamics of the polymer segments at the inorganic interfaces, all indicate that this filler configuration enhances the polymer-ceramic interfaces. Polarization as a function of electric field and dielectric breakdown show improvements in the electrical properties of these composites, compared to the corresponding unfilled epoxy, despite the expected reduction in crosslinking density. The resulting nanocomposites have a property set which can be utilized in energy storage and power system applications. © *2010 American Institute of Physics*.
[doi:10.1063/1.3487471]

I. INTRODUCTION

The design of high performance power systems necessitates novel dielectric materials with enhanced insulating properties. Toward this direction, polymer nanocomposites have been extensively investigated in an effort to improve the electrical insulation[1–6] and the thermomechanical properties[7–13] of the polymer matrix. The main drawbacks in such approaches typically relate to the polymer-filler interfaces, in particular when these interfaces are characterized by properties adverse to the desired macroscopic behavior. With increasing filler surface area, and depending on the polymers-filler interactions,[14,15] the presence of such interfaces can govern the macroscopic properties of the composite[16] and also determine properties like the impact strength[7–13] or the dielectric breakdown strength.[17,18]

In the previous paper of this series,[19] we investigated epoxy resin composites based on organically modified montmorillonite (oMMT) and barium titanate (BT) nanoparticles in order to exploit the high aspect ratio of the montmorillonite (MMT) and the high permittivity of the BT particles, which improve the mechanical performance and the operating electric field of the nanocomposite, respectively. The interfacial properties were found to dominate the dielectric performance of these composites at 3 wt % of oMMT and above 10 vol % loadings of BT. In addition, the dynamics of the polymer at the MMT interfaces were found to be approximately three orders of magnitude slower than those at the BT interfaces, indicating more robust interfaces in the MMT composites than in the BT-based composites (the corresponding energy barriers (activation energies) associated with these motions were also double for the MMT systems). Finally, a dual-filler composite—consisting of epoxy reinforced by both oMMT and BT nanofillers—was also studied, showing limited synergy between the two fillers. However, those dual-filler composites showed a phase-separated morphology, with regions largely containing only oMMT agglomerates or only dispersed BT fillers.[19]

Herein, in order to better integrate the good properties of the two distinct nanofillers, we covalently-bonded oMMT and BT nanoparticles by appropriately modifying the surface of the fillers, with multiamines and epoxide-containing silanes, respectively. Subsequently, composites were obtained by dispersing these covalently-bonded "hybrid" fillers in an epoxy resin matrix, at several filler concentrations. Transmission electron microscope (TEM) images illustrate a unique spatial configuration of spherical BT particles being surrounded by attached layered oMMT particles. The epoxy-matrix curing process, particularly the concentration of the crosslinker, was optimized by accounting for the reactive organic treatments of the fillers. Emphasis was further given on the polymer-ceramic interfacial properties: The covalently-bonded inorganic particle configuration was found to enhance the polymer-filler interfaces, resulting in significant improvements of the dielectric and mechanical properties. Finally, we assessed the suitability of the composites for

a)Electronic addresses: manias@psu.edu and car4@psu.edu.

power applications by investigating the dielectric losses under high electric fields and the dielectric breakdown strength of the system.

II. EXPERIMENTAL

A. Materials

The preparation of the covalently-bonded $BaTiO_3$/oMMT particles was implemented in two steps. First, Na^+-MMT clay was modified with ammonium-based aliphatic surfactants and the $BaTiO_3$ particles were surface treated with epoxide terminated ethoxy silane coupling agents. Subsequently, bonding of the fillers was achieved by mixing the two in a solution under conditions that promoted reaction between the two organic modifications.

Specifically, for the MMT surface modification, 10 g of Na^+-MMT clay (Nanocor Inc.) with nominal cation exchange capacity (CEC) of 1.45 meq/g were dispersed in 300 ml deionized water (20 MΩ) and the suspension was stirred for 30 min at 70 °C, resulting in a stable suspension with no visible clay aggregates. In a second beaker, 16.5 mmol of octadecyl-amine (Sigma Aldrich), which corresponds to 150% excess of the CEC value, and stoichiometric quantity of hydrochloric acid HCl (for protonating the amines toward ammoniums), were added to 300 ml of ethanol, and after stirring for 30 min the temperature was increased to 70 °C. In a third beaker, 4.5 mmol of an aliphatic amine [triethylene tetramine (TETA) in *purum* form, Air Products and Chemicals] and 4.5 mmol of HCl were dissolved in ethanol and stirred for 30 min at 70 °C. The TETA solution in the third beaker was added to the second beaker, and the combined two-surfactant solution was added to the clay suspension in the first beaker (flocculation of excess surfactant and white organoclay precipitation were observed immediately upon mixing). The reaction was allowed to completion under vigorous mixing for two hours, before the modified clay was paper-filtered and washed three times in ethanol until all excess surfactant not coulombically-bound on the MMT was removed (as indicated by a clear silver-nitrate test). The obtained powder was dried in a vacuum oven for 12 h at 80 °C and was found to have approximately 32 wt % end-tethered ammonium organics [as quantified by thermogravimetric analysis (TGA), cf. Fig. 2].

For the surface treatment of the second component, $BaTiO_3$ particles in powder form (hydrothermal BT-8, Cabot Performance Materials, Boyertown, PA having a Ba/Ti ratio of 0.998 and a median particle size of 150 nm) were modified with (3-glycidoxypropyl)trimethoxysilane (Gelest) as follows: 12 g of purified (leached) BT powder were suspended in a solution of 90 ml ethanol, 10 ml distilled water, and 0.6 g of (3-glycidoxypropyl)trimethoxysilane. The obtained mixture was stirred for 24 h, subsequently centrifuged for 10 min and finally the precipitated modified powder was dried at 120 °C for 6 h. The two organically modified nanoparticulate components were mixed in a weight ratio $W_{BT}:W_{oMMT}=2:1$ and allowed to react in a methanol solution under ball-milling for 24 h.

Composites were prepared by adding the fillers into an epoxy resin (diglycidyl ether of bisphenol-F, Epon 862, Hexion Specialty Chemicals). The dispersion of the particles was improved by high shear mixing and sonication of the suspension. The suspensions were charged with appropriate amounts of crosslinker, 2-ethyl-4-methylimidazole (Curing Agent Imicure™ EMI-24), and were degassed under vacuum to remove any trapped air voids. Films 100 μm thick were obtained by casting the solutions between teflon plates and placing them on a hot plate to accelerate the curing process [the samples were cured at 60 °C for 3 h and post-cured at 180 °C (Ref. 19)].

B. Instrumentation

1. Transmission electron microscopy

A Leica Ultracut UCT Microtome with cryoattachment was used for sectioning the specimens. The microtomed samples were tested under a TEM (Jeol JEM-2010 with LaB_6 emitter) operated at an accelerating voltage of 200 kV.

2. TGA

TGA measurements were performed on a Thermal Analysis (TA) Instruments SDT-Q600 analyzer under nitrogen environment. The temperature ramps were from 20 to 1000 °C at a heating rate of 10 °C/min.

3. Differential scanning calorimetry (DSC)

DSC data were collected on a TA Instruments Q200 calorimeter in a gas mixture of nitrogen and helium. The measured heat flow was obtained in the conventional mode at a cooling temperature ramp of 5 °C/min. The temperature uncertainty was ±0.1 °C. For monitoring the glass transition, high to low temperature ramps, with or without temperature modulation, were performed in order to follow the same thermal sequence as in the dielectric spectroscopy experiments. The postcuring temperature of the specimens was defined by the completion temperature of the epoxy matrix curing reaction.[19] For the data analysis, the TA universal analysis software was used.

4. Dynamic mechanical analysis (DMA)

DMA measurements were carried out on a TA Instruments Q800 instrument. Sample strips (15 mm in length, 6 mm in width, and 200 μm thick) were measured in the tensile mode at a frequency of 1 Hz. The temperature ramps were performed under 1 MPa stress (well within the linear region in the stress-strain curves) and at a 4 °C/min heating rate.

5. Dielectric relaxation spectroscopy (DRS)

DRS experiments were performed over a broad frequency (10^{-2} to 10^6 Hz) and temperature (180 to 30 °C) range. Disklike specimens, about 100 μm thick and 20 mm in diameter, were sandwiched between gold-sputtered brass electrodes and mounted on a Novocontrol ZGS Alpha active sample cell, which was connected to a Novocontrol Quatro Cryosystem for temperature stabilization (±0.1 °C). Prior to the DRS measurements, the samples were equilibrated in the cell at 100 °C for 30 min to eliminate bulk water contribu-

tions to the spectra and to facilitate similar conditions in all systems measured. The real and imaginary parts of permittivity [$\varepsilon^*(\omega)=\varepsilon'(\omega)-i\varepsilon''(\omega)$, ω is the angular frequency] were collected isothermally in the order of decreasing temperature. A detailed description of the data analysis has been presented elsewhere.[20–22]

6. Displacement-electric field loops

High-field polarization-electric field loops were recorded with a modified Sawyer–Tower circuit. The samples were subjected to two successive sine waves, with frequency of 1 Hz. The polarization-electric field loops are presented according to the data from the second cycle.

7. Dielectric breakdown strength

Dielectric breakdown measurements were performed on a TREK P0621P instrument. The samples were sandwiched between a one-side conducting polypropylene tape (top electrode) and a copper plate (bottom electrode). All the specimens were tested at room temperature under a dc voltage ramp of 500 V/s (more details can be found elsewhere[23]).

III. RESULTS AND DISCUSSION

A. Structural analysis

Transmission electron microscopy was employed to reveal the fillers' structure and their dispersion within the polymer matrix. When unmodified BT and organically modified silicates were simply mixed and dispersed in the epoxy resin, the resultant composite structure was a phase-separated morphology that consisted of regions with predominately one filler type: Namely, those composites showed distinct regions with dispersed and agglomerated oMMT and regions with dispersed $BaTiO_3$ particles [Fig. 1(a)]. In contrast, under the same filler dispersion method, the covalently-bonded $BaTiO_3$/oMMT hybrid nanoparticles exhibit a much more uniform dispersion throughout the polymer matrix [as demonstrated by TEM imaging, Fig. 1(b)]. In addition, the covalent bonding between BT and oMMT not only altered the composite morphology—filler dispersion—but also gave rise to a unique filler architecture: Specifically, tactoids of a few layered silicates (~5–30 nm thick, cf. two to ten epoxy-intercalated oMMT layers) are attached to the outer surface of the spherical $BaTiO_3$ particles (~150 nm in diameter) constructing hybrid nanoparticles [Figs. 1(c)–1(f)], which in turn were randomly dispersed in the polymer (epoxy) matrix, as dictated by the favorable epoxy-oMMT interactions [Fig. 1(b)].

This spatial configuration of the hybrid fillers, minimized the area of the "unfavorable" interfaces and improved the uniformity in filler dispersion, and is thus expected to maximize the good properties of both fillers.[16] In particular, it is expected to combine more synergistically the high permittivity value of the BT particles—compared to the low permittivity of the polymer and the oMMT—with the good interfacial properties of the reactive-oMMT fillers. The latter, due to the high MMT surface area and due to the filler-filler bonding and configuration, is also anticipated to effectively shield the dielectrically weaker polymer-BT interfaces.[19] In addition, and depending on the exfoliation degree of the oMMT phase, this dispersed inorganic phase may also contribute an improvement of the dielectric breakdown strength of the nanocomposites by forming a space-charge dissipating layer.[24]

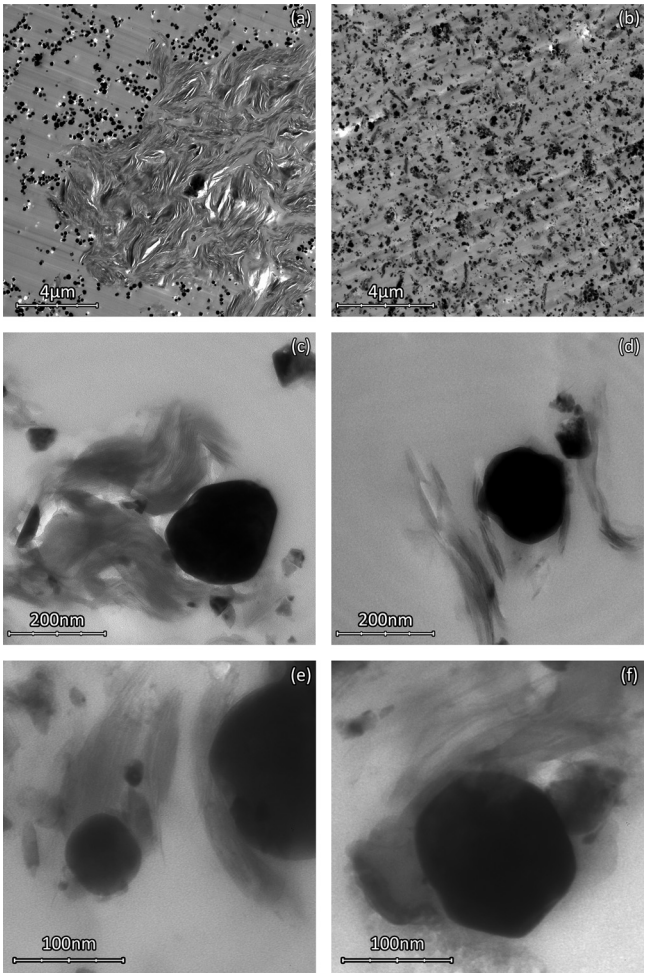

FIG. 1. TEM images of the $BaTiO_3$/oMMT based nanocomposites: (a) low magnification of a composite with noncovalently-bonded BT and oMMT, at 10 vol % BT and 3 wt % oMMT. (b) Low magnification of a composite with 20 wt % hybrid fillers, i.e, BT covalently-bonded with reactive oMMT at 2:1 BT:oMMT ratio. The two composites shown in (a) and (b) have essentially the same components and differ only in the filler bonding; comparing the two, it becomes clear that covalent-bonding of the BT and oMMT nanoparticles leads to a substantially better dispersed composite morphology. TEMs (c) through (f) are higher magnification images of the covalently-linked BT/oMMT nanofillers in the same nanocomposite as shown in (b).

The organic content of the modified inorganic constituents was determined by employing TGA and the corresponding curves are presented in Fig. 2. In the high temperature limit, the weight-loss plateau values estimate the organic fraction in each nanofiller, which is approximately 3 wt % and 32 wt % for the BT and the oMMT, respectively. The last is in good agreement with the organic weight fraction of a commercial oMMT (Nanocor I.30E), which contains the same MMT (same size and CEC) but is modified only with octadecyl-ammonium surfactant. For the hybrid covalently-bonded BT/oMMT fillers, the organic content is around 15 wt %, which is close to the estimated value according to the

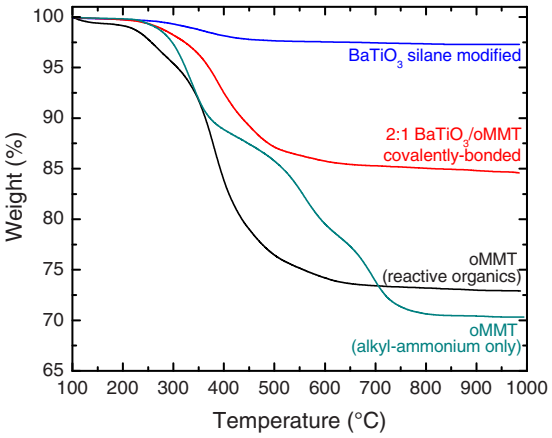

FIG. 2. (Color online) Thermogravimetric analysis curves, in nitrogen atmosphere, of the covalently-bonded $BaTiO_3$/oMMT fillers along with the individual organically modified constituents: $BaTiO_3$ particles after surface modification with (3-glycidoxypropyl)trimethoxysilane, and oMMT with mixed (TETA and octadecyl-ammonium) surfactants; for comparison, oMMT particles with octadecyl-ammonium only surfactants are also shown for the same MMT. Weight losses were normalized at 100 °C to account for any solvent evaporation; the ultimate weight loss corresponds to the total organic content of each nanofiller.

2:1 weight ratio of the two fillers used (see Sec. II A). Considering the configuration of these hybrid oMMT/BT particles [Figs. 1(c)–1(f)] and the significantly higher concentration of amine-based surfactants on the oMMT compared to the epoxide silanes on the BT particles, it is expected that unreacted amine groups (TETA) will exist in considerable amounts at the organic-inorganic interfaces. These MMT-bound unreacted TETA molecules will readily react (crosslink) with the epoxy matrix under the conditions used here. In order to account for this population of unreacted TETA surfactants, and thus to achieve a maximum crosslinking density at the interfaces, we had to optimize the concentration of the added curing agent (EMI-24) that was used for crosslinking the epoxy resin in the composites.[25] For that reason, the effect of the curing agent concentration on the macroscopic glass transition of the composites was investigated and a detailed analysis follows.

The DSC thermograms of the sample with 15 wt % in covalently-bonded BT/oMMT filler, over a wide concentration range for the curing agent, are shown in Fig. 3(a) (dotted lines), and the corresponding glass transition temperatures are summarized in Fig. 3(b). The glass transition temperature, T_g, is found to shift toward higher temperatures with increasing curing agent concentration. A maximum value (~138 °C) is observed, at approximately 70 wt % of the curing agent's stoichiometric amount for the unfilled resin, followed by a decrease in T_g at higher curing agent concentrations [Fig. 3(b)]. In the system under investigation, this experimentally obtained curing agent concentration[25] (70 wt % of the stoichiometric amount for the matrix) was normalized by the filler weight fraction and was subsequently used as the optimum concentration, i.e., achieving full matrix crosslinking while minimizing the presence of unreacted curing agent or unreacted epoxide groups. Both these unreacted species would lead to the formation of mobile moieties in the polymer network which, in turn, would decrease the glass transition temperature [cf. composite formulations deficient in or with excess of amine groups, Fig. 3(b)], and may also

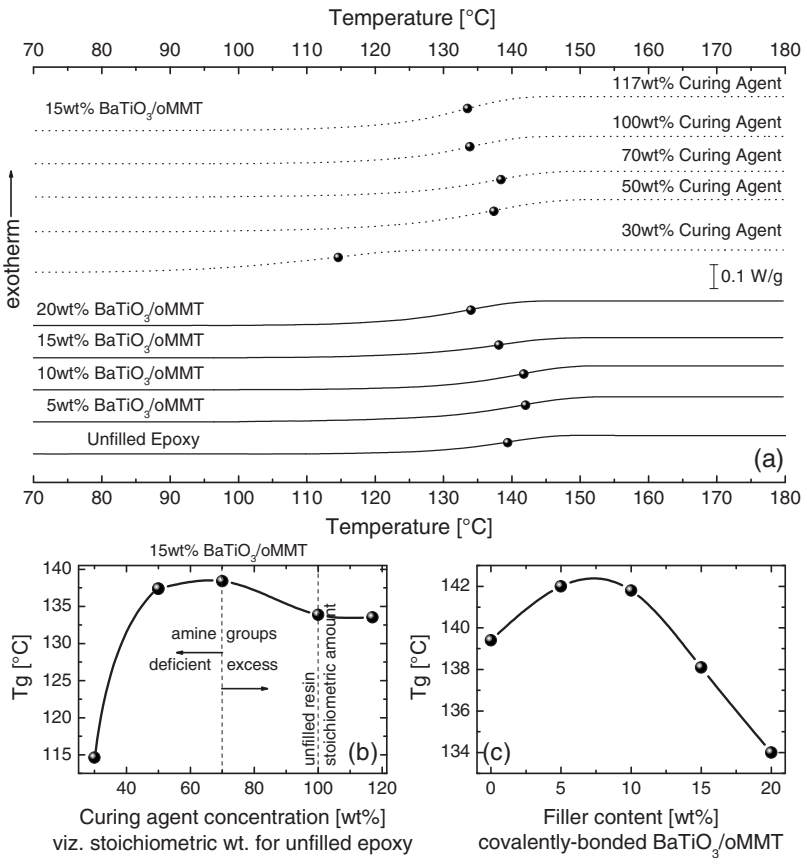

FIG. 3. (a) Vertically shifted DSC curves (after baseline subtraction) of the nanocomposites with several concentrations of covalently-bonded $BaTiO_3$ and oMMT particles (solid lines, bottom). For the 15 wt % composite the dependence on the curing agent (EMI-24) concentration is also presented (dotted lines, top), where 100 wt % corresponds to the stoichiometric amount needed for the unfilled epoxy. The solid spheres depict the glass transition temperatures. (b) The dependence of T_g on the curing agent concentration for the 15 wt % covalently-bonded $BaTiO_3$/oMMT composite. (c) The dependence of T_g on the filler weight fraction (covalently-bonded $BaTiO_3$/oMMT). In (b) and (c) the lines are guides for the eye; all data were collected at a cooling temperature ramp of 5 °C/min; the uncertainty in the T_g values is ±1 °C depending on baseline and fitting.

TABLE I. Summary of DSC and DMA results for epoxy and its composites with hydrid (covalently-bonded) BT/oMMT fillers.

Sample	T_g^{DSC} [a] (°C)	ΔC_p^* [b] (J/g °C)	ΔT [c] (°C)	T [d] at G''^{peak}_{DMA} (°C)	T [e] at δ^{peak}_{DMA} (°C)	$\Delta G'_{35C}$ [f] (%)
Unfilled epoxy	139.4	0.17	15.9	143.9	150.9	···
5 wt % $BaTiO_3$/oMMT	142.0	0.21	18.8	144.7	152.0	39
10 wt % $BaTiO_3$/oMMT	141.8	0.20	19.4	141.3	148.2	53
15 wt % $BaTiO_3$/oMMT	138.1	0.18	19.8	135.0	142.3	68
20 wt % $BaTiO_3$/oMMT	134.0	0.26	18.8	133.1	140.4	42

[a] T_g^{DSC} is the calorimetric glass transition temperature (the error is ±1 °C).
[b] ΔC_p^* is the change in heat capacity per epoxy mass: $\Delta C_p^* = \Delta C_p/(1-X)$, where ΔC_p is the measured value (per mass of sample) and X is the weight fraction of the BT/oMMT filler (the error is ±0.2 J/g °C).
[c] $\Delta T = T_{onset} - T_{end}$ is the temperature width of the glass transition process. T_{onset} and T_{end} are the temperatures corresponding to the beginning and the completion of the process, respectively.
[d] T at G''^{peak}_{DMA} is the temperature at the loss modulus maximum, associated to the apparent T_g.
[e] T at δ^{peak}_{DMA} is the temperature corresponding to the tan δ peak maximum, defining the apparent T_g.
[f] $\Delta G'_{35C}$ is the relative change in storage modulus at 35 °C compared to the unfilled epoxy.

decrease the dielectric breakdown strength of the nanocomposites due to a possible increase in the local polarization. The 15 wt % in BT/oMMT was chosen for optimizing the curing agent concentration through this DSC study, since it yielded a sensitive dependence of T_g on the curing agent concentration.

In view of the above, and taking into account the dependence of the T_g on the polymer-filler interactions and on the filler dispersion,[26,27] we investigated the thermodynamic properties of the fabricated nanocomposites. The DSC thermograms for all composites are presented in Fig. 3(a) (solid lines) and the T_g dependence on the filler weight fraction is shown in Fig. 3(c) (the respective data are summarized in Table I). With respect to the T_g values of the unfilled epoxy, addition of 5 and 10 wt % filler shifted the T_g to higher temperatures,[26,28] whereas the 15 and 20 wt % composites shifted T_g to lower temperatures. The T_g decrease at high loading filler levels is much less pronounced than in epoxy/oMMT systems with comparable contents of MMT.[29,30] In addition, the *per polymer mass heat capacity change* (ΔC_p^*) for the composites at 5, 10, and 15 wt % is similar (within the errors) to that of the unfilled epoxy matrix (Table I). This is a strong indication that the composites and the neat epoxy network are both characterized by similar crosslinking density. The ΔC_p^* value for the 20 wt % composite is slightly higher, which may originate from reaching the filler percolation limit, and thus relate to the initiation of appearance of weak interfaces where the polymer chains are more mobile[31] (more details on the correlation between the heat capacity and the mobility of the polymer chains can be found in literature[32,33]). Moreover, for all composites the width of the glass transition process (ΔT) is comparable to that of the respective unfilled epoxy. Albeit the polymer-ceramic boundaries and interfaces, the DSC results suggest that the local environments that contribute to the glass transition are homogeneous and resemble those in the unfilled epoxy. The above thermodynamic properties of the glass transition process are consistent with the development of robust interfaces (e.g., T_g increases for filler weight fractions below the percolation threshold limit), which can only emanate from the crosslinking between the TETA on the oMMT particles and the epoxides in the polymer matrix, and which are thermodynamically similar to the bulk environments.[13,34] These T_g based insights on the interfacial strength of the composites will be correlated with the composites' mechanical and electrical properties in the following sections.

Dynamic mechanical analysis was also performed to investigate the thermomechanical properties of the composites and their relationship to the electrical properties. The tan δ, storage modulus (G'), and loss modulus (G'') plots for all the samples over a wide temperature range, are presented in Fig. 4. At temperatures lower than the glass transition temperature (glassy state), all the composites exhibit higher G' values compared to the respective unfilled matrix. For the 5, 10, and 15 wt % BT/oMMT composites, G' is found to increase systematically with the filler weight percent for all temperatures below T_g. Further increasing the filler loading to 20 wt % shows a decrease in the storage modulus, which is in good agreement with the thermodynamic properties dis-

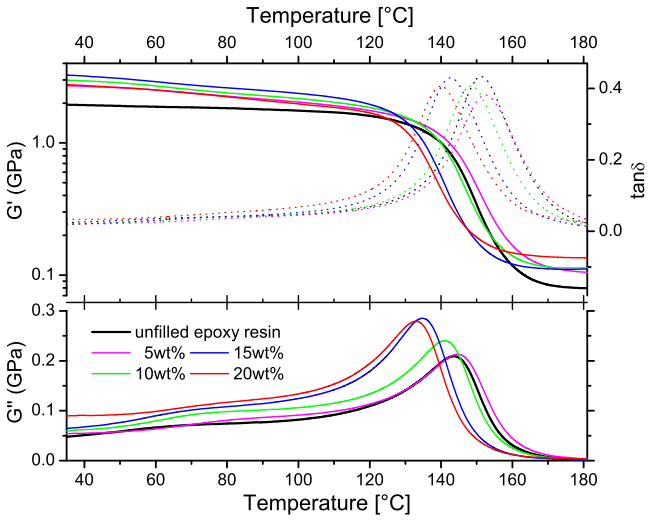

FIG. 4. (Color online) Dynamical mechanical analysis results: storage (G') and loss (G'') moduli, and tan δ of the unfilled epoxy resin compared with the covalently-bonded $BaTiO_3$/oMMT nanocomposites (all measurements were performed at 1 Hz deformation and 4 °C/min heating rate; filler weight fractions as indicated in the plot).

cussed previously, i.e., consistent with crossing the filler percolation threshold and with the decrease in T_g.

At 35 °C the relative change in G' of the nanocomposites compared to the respective unfilled epoxy, are summarized in Table I. For all composites this low temperature storage modulus is increasing (by 39% to 68%) and the 15 wt % composite exhibits the maximum increase, approximately by 68%. For the same temperature, and taking into account the weight ratio of the fillers ($W_{BT}/W_{oMMT}=2$), the composites based on covalently-bonded BT/oMMT exhibit a significant improvement in the G', compared to respective epoxy composites with a single filler at the same concentration, either oMMT (Refs. 30 and 35) or BT.[36] In the temperature region 50 to 100 °C, a weak relaxation process manifests in the loss modulus in Fig. 4 (an associated, albeit weak, step is also present in the storage modulus). This mode is more pronounced in the nanocomposites, whereas in the unfilled resin is almost negligible. This type of relaxation typically arises during the annealing of small residual stresses within the polymer network. The curing and postcuring thermal cycles determine the intensity and the position of this relaxation, which evidently reflects here stresses in the epoxy locked-in during the 60 °C curing. However, since all specimens were prepared under the same thermal process, the observed variation in this mode with the filler loading can be ascribed to structural changes (cf. changes in interfacial area). Apparently in the nanocomposites residual stresses and heterogeneities in the crosslinking density become more prominent due to the polymer-filler interfacial areas, and thus these relaxations can be attributed mainly to a polymer phase in the immediate vicinity of the fillers (viz. polymers tightly bound on the filler surface[37,34] that may exhibit different crosslinking density compared to the bulk phase). This filler-bound polymer phase is increasing with filler loading and manifests in higher intensity of the loss peak, as shown in Fig. 4. Interestingly, any changes in the DSC heat capacity due to this interfacial polymer phase are within the errors for concentrations below 15 wt %, which indicates that this relaxation is thermomechanical, rather than thermodynamic, in nature.

At higher temperatures the storage modulus decreases, manifesting a rubbery state for the epoxy and the composites. The accompanied relaxation is associated to the *apparent glass transition* and this apparent T_g can be defined as the temperature which corresponds to the peak maximum of the loss modulus (or of the tan δ). These values are also summarized in Table I and their variation with the filler loading is in good agreement with that derived from the DSC scans [the T_g values based on the G'' peak are closer to the calorimetric values than those based on the tan δ (Ref. 38)]. Both techniques, calorimetric and thermomechanical, indicate a nonmonotonic dependence of the glass transition temperature on the filler content. At low loadings the T_g—either thermodynamic or apparent—is increasing, whereas for higher loadings it is decreasing (quantitatively, even at the highest filler loading (20 wt %) the T_g reduction is less than 10 °C). Our previous studies on composites with a single inorganic phase (either BT or oMMT) showed a monotonic and far more pronounced decrease in the T_g values, even at low filler loadings.[19] In this work, the higher T_g values are reflecting the enhancement of the polymer-filler interfaces due to the reactive nature of the oMMT organic modification.

Finally, in Fig. 4 at temperatures above the completion of the glass transition process, the loss modulus is approaching a zero value, and the storage modulus reaches its plateau value. For all composites, this plateau modulus is higher than for the unfilled epoxy, indicating that the fillers strengthen the rubbery network responsible for the viscoelastic behavior, i.e., acting to increase the *effective* polymer crosslinking or entanglements (cf. entanglements can be considered as transient crosslinks). The composites' plateau moduli seem to adopt two values (one for low filler loadings and another value for the 20 wt % filler, which is above the percolation concentration) a behavior which, assuming the typical plateau modulus scaling ($G'_e \propto \rho RT/M_e$), indicates that the plateau modulus is determined by the sorbed polymer on the fillers or by a polymer-stabilized filler network,[39] rather than any filler-induced changes in crosslinking density. In the latter case, since the oMMT are reactive and can participate in the crosslinking of the epoxy matrix, increasing the filler concentration would lead to a proportional increase in crosslinking density, which, it turn, would lead to a systematic increase in the plateau modulus (a trend which is clearly not observed in the DMA data in Fig. 4).

B. Dielectric properties under low electric field

Dielectric relaxation spectroscopy was performed on the nanocomposites in a broad temperature and frequency range. In the glassy state (room temperature to glass transition temperature) the 5, 10, and 15 wt % composites did not show any pronounced dielectric relaxation modes, whereas the 20 wt % composite exhibits a relaxation mechanism [Fig. 5(a)]. The analysis of this mode was carried out in the permittivity interpretation by employing a Havriliak–Negami expression and a conductivity contribution:[40,41]

$$\varepsilon^*(\omega) = \varepsilon_\infty + \frac{\Delta\varepsilon}{[1+(i\omega\tau_o)^{1-\alpha}]^\beta} - i\frac{\sigma_o}{\varepsilon_o}\omega^{-s}, \quad \begin{cases} 0 \le \alpha < 1 \\ 0 < (1-\alpha)\beta \le 1 \\ 0 \le s \le 1 \end{cases}, \tag{1}$$

where τ_o is the characteristic time related to the frequency of the loss peak maximum; α and β are the shape parameters of the loss peak; $\Delta\varepsilon$ is the dielectric relaxation strength ($\Delta\varepsilon = \varepsilon_s - \varepsilon_\infty$); ε_s and ε_∞ are the low and high frequency limits of the $\varepsilon'(\omega)$ function; and σ_o and ε_o stand for the conductivity contribution and the permittivity of free space, respectively (details of the fitting analysis procedure have been given in detail elsewhere[20,21]).

The temperature range of this relaxation mechanism is in good agreement with the temperature range of the weak mode seen in the DMA plot, cf. Fig. 4. In the composites with lower filler loading this mode is absent in DRS, although it was observed in the DMA measurements. This is probably due to the weak dielectric relaxation strength of the process ($\Delta\varepsilon \sim 1$ for the 20 wt % composite), which allows

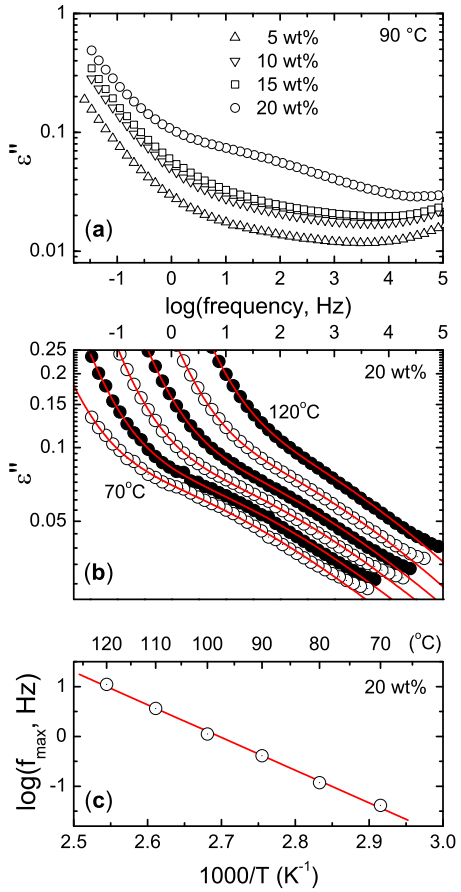

FIG. 5. (Color online) Dielectric relaxation spectroscopy data below the T_g. (a) Dielectric loss curves for the nanocomposites with hybrid (covalently-bonded) $BaTiO_3$/oMMT, for various filler loadings (5 to 20 wt %). A relaxation process is clear only for the highest (20 wt %) filler loading composite, and this mode is ascribed to the formation of a polymer phase loosely-bound to the inorganic filler surfaces; based on the DMA results, this mode is present also in the other—lower filler loading—composites but does not manifest here in ε'', probably due to its weak dielectric relaxation strength. (b) Dielectric loss curves for the 20 wt % nanocomposite at the temperature range 120–70 °C in steps of 10 °C; the lines are the best fits of Eq. (1) to the experimental data. (c) The corresponding Arrhenius plot of the loss peak maximum frequency, i.e., of the relaxation rate of the sub-T_g mode.

the low frequency conductivity contribution to mask this relaxation peak for the smaller filler loadings. Since $\Delta\varepsilon$ is proportional to the density of the relaxing units and their dipole moment,[41] this sub-T_g mode can be ascribed to the formation of a polymer phase that is loosely bound to the inorganic surfaces (near the fillers but more mobile than the sorbed polymers,[34,37,42] cf. DSC results). For filler loadings below the percolation threshold, there evidently exist less mobile interfaces (i.e., a more tightly bound phase, see also ΔC_P^* values in Table I) and the number density of the relaxing units decreases. Both these trends are in agreement with the DSC observations and, in combination, they result in a weak $\Delta\epsilon$ for this mode, which cannot be detected. The characteristics (strength and dynamics) of this relaxation can be used as an indirect measure of the polymer-filler interfacial strength. In our previous work[19] we reported the interfacial dielectric properties of epoxy nanocomposites based on either BT, or oMMT, or both fillers but unreacted. In the same temperature range, DRS relaxations arising from the interfaces were pronounced even at low filler concentrations,[19] whereas in this system–with covalently-bonded BT/oMMT fillers–the interfacial relaxation is present in the DRS for only the highest filler concentration.

For the 20 wt % content the loss peak maximum frequency (f_{max}) was obtained from the best fit of Eq. (1) to the experimental data in Fig. 5(b). The dependence of f_{max} versus the reciprocal temperature is shown in Fig. 5(c) and is described well by the Arrhenius equation:[41]

$$f_{max}(T) = f_\infty \exp\left(-\frac{E_A}{k_B T}\right), \tag{2}$$

where f_∞ is the relaxation rate in the high temperature limit; k_B is the Boltzmann's constant; and E_A is the corresponding activation energy (which can be determined from the best linear fit of Eq. (2) to the data in Fig. 5(c) and was found to be 226 kJ/mol).

Compared to the respective single-filler composites,[19] this value is approximately 20% higher than the activation energy for the corresponding epoxy/oMMT composites and 150% higher than the E_A value for the epoxy/BT composites. Furthermore, the dynamics in Fig. 5(c) are approximately 1.5 and 4.5 orders of magnitude slower than in the oMMT and BT composites, respectively.[19] Both the dramatically slower dynamics, as well as the higher energy barriers associated with this relaxation, manifest a marked improvement of the polymer-filler interfacial strength in the epoxy/BT/reactive-oMMT system, even for filler loadings above the percolation limit. This is a strong indication that the TETA amine groups on the oMMT surfaces reacted also with the epoxide groups in the epoxy matrix, in addition to reacting with the epoxides on the BT fillers covalently bonding the two types of nanoparticles.

At temperatures above the T_g, all the composites exhibit a plateau in the low frequency regime of the ac conductivity (i.e., a dc conductivity, σ_{dc}) and a comparison plot at a representative temperature (160 °C) is shown in Fig. 6(a). The 5 wt % sample reveals a dc conductivity value which is lower than the value of the pristine epoxy matrix. Further increase in the filler content (10, 15, and 20 wt %) leads to a systematic increase in the σ_{dc}.

In the rubbery state, the conductivity mechanism is inherently connected to the glass transition temperature of the polymer matrix and to the mobility of the polymer chains at the interfaces. In order to separate these two contributions the temperature in the Arrhenius plot of the dc conductivity was normalized by the corresponding calorimetric glass transition temperature [Fig. 6(b)], as per.[43] Two distinct behaviors are observed: The 5 wt % composite and the unfilled epoxy exhibit the same dependence; this is an indication that at this low filler content the contribution of the interfaces to the conduction mechanism is negligible. However, for the composites with 10, 15, and 20 wt % filler, the conductivity increases approximately five times. This increase is arising from the polymer-filler interfaces, which evidently dominate the conduction process for temperatures higher than T_g, even for filler concentrations below the percolation threshold. Similar behavior is observed in the activation energy values of the conduction mechanism, shown in Fig. 6(c). The 5

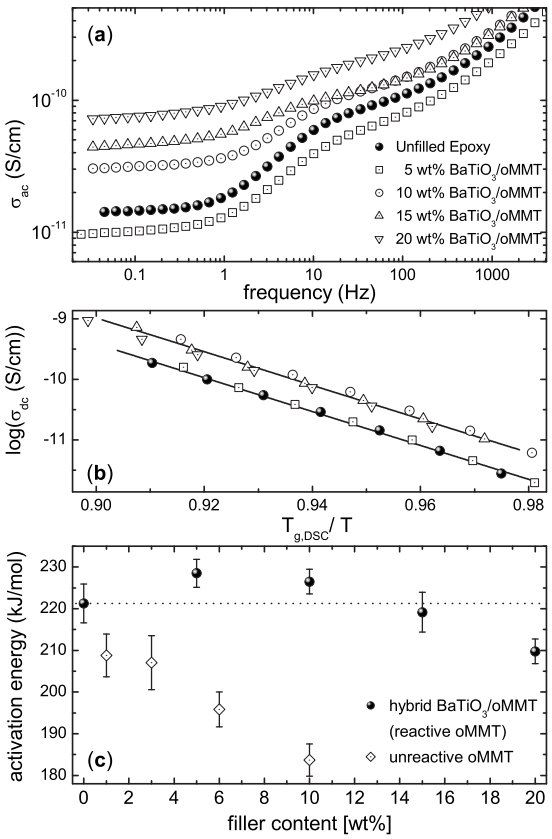

FIG. 6. Dielectric relaxation spectroscopy data above the T_g. (a) DRS conductivities for the unfilled epoxy and the nanocomposites based on covalently-bonded BT/oMMT nanofillers at 160 °C. The feature (step) at frequencies higher than the onset of dc conductivity (1–10 Hz) is related to Maxwell–Wagner–Sillars effects; a detailed discussion can be found in Ref. 19. (b) The corresponding Arrhenius plot of the dc conductivity values normalized by each system's calorimetric T_g. The σ_{dc} values were obtained at 0.04 Hz and the lines are the best linear fits to the unfilled epoxy and to the 15 wt % nanocomposite. (c) The activation energies calculated from Eq. (2) (solid symbols). For comparison the activation energies of epoxy resin nanocomposites with similar loadings of nonreactive oMMT are also shown (open symbols, Ref. 19).

wt % exhibits the highest value and a systematic decrease is observed upon filler content increasing. However, all the BT/oMMT composites exhibit higher E_A values compared to the respective epoxy composites with oMMT,[19] clearly manifesting that the enhancement of the interfaces is due to the crosslinked filler configuration and to the reactive (TETA) organic modification of the oMMT. The above discussion is assuming no appreciable increase in the dc conductivity due to an increased space-charge with higher filler loadings; this is a reasonable assumption since the fillers are not expected to introduce high populations of *free* ions that could contribute to space-charge effects. Finally, the DRS spectra for temperatures above the T_g show a relaxation at frequencies above the onset of dc conductivity (1–10 Hz) across all systems. This relaxation is associated to space-charge, it is Maxwell–Wagner–Sillars in nature (cf. $\Delta\varepsilon \sim 16$ for 5 wt % composite at 160 °C), and it follows the dependencies of the dc conductivity. The origins of this process have been investigated, in terms of the modulus formalism for essentially the same interfaces, in the first of these two-paper series.[19]

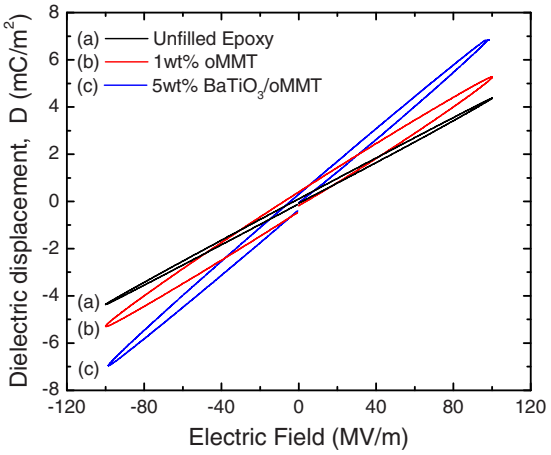

FIG. 7. (Color online) Comparative dielectric displacement vs electric field (*D-E* plots) indicating low losses and high permittivity for the composite with 5 wt % in covalently-bonded BT/oMMT nanofillers (curve c). These composites show a markedly enhanced performance compared to the respective unfilled matrix (curve a), as well as better performance than the composites with similar concentration of nonreactive oMMT (curve b).

C. Dielectric properties under high electric fields

1. Displacement-electric field loops

The electrical properties of the composites exhibit a strong dependence on the amplitude and frequency of the applied electric fields.[21,44,45] Fillers with high permittivity create dielectric inhomogeneities within the composite. This increases the local field concentration at the filler-polymer interface, due to the contrast between the permittivity and the conductivity of the two phases. In the first paper of this series,[19] we demonstrated the role of the interfaces in controlling the dielectric breakdown strength and the recoverable energy density of these type of composites under high electric fields. It is therefore vital to understand how the reactive fillers change the high field losses in the present systems, which arise, primarily, from dc conduction and space charge. Here, we study the shape of the polarization-electric field curves to quantify the behavior of these systems at high fields. We present comparative results for the unfilled epoxy, the 5 wt % covalently-bonded BT/oMMT composite, and the 1 wt % oMMT nonreactive single-filler composite (which is an epoxy/oMMT nanocomposite with good filler dispersions and comparable oMMT concentration as the 5 wt % BT/reactive-oMMT).

The dielectric displacement-electric field (*D-E*) loops as a function of electric field are shown in Fig. 7. The widening (or opening) of the loops shows a deviation from the linear behavior of the dielectric displacement versus the electric field ($D=\varepsilon_o\varepsilon' E=\varepsilon_o E+P$, where P is the polarization) and can be related to the losses present in the system. A linear behavior of the dielectric displacement with the applied field was observed at all field strengths for the unfilled epoxy. It is interesting to note that the *D-E* loop for the 5 wt % BT/oMMT composite depicts very minimal widening, even at high fields up to 10^8 MV/m. This behavior is different compared to the respective nonreactive dual-filler epoxy/BT/nonreactive-oMMT systems, cf. Fig. 1(a), and is also different to the respective single-filler (epoxy/BT or epoxy/

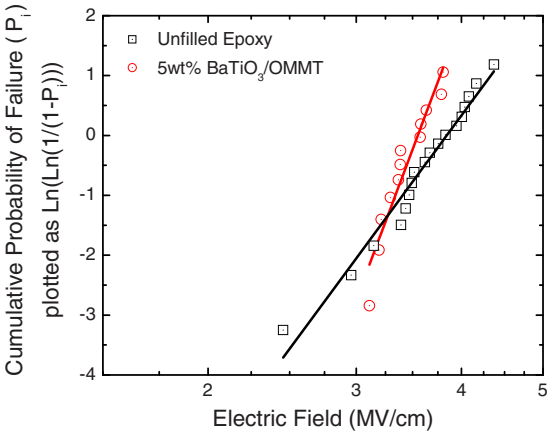

FIG. 8. (Color online) Weibull plot depicting the cumulative breakdown probability distribution as a function of applied field; the unfilled epoxy and the respective composite with 5 wt % of covalently-bonded BT/oMMT nanofillers are compared (solid lines are the Weibull predictions).

oMMT) composites reported before.[19] A comparison between the unfilled epoxy, the 1 wt % oMMT composite, and the 5 wt % BT/reactive-oMMT, shows the highest losses for similar fields in the 1 wt % oMMT composite, as discussed before.[19] Also, the slope of the *D-E* loop for the 5 wt % BT/oMMT indicates a higher permittivity at high *E*-fields without increasing the high-field losses, compared to all other systems. The superior performance of the 5 wt % BT/reactive-oMMT is consistent with the higher T_g value (Fig. 3 and Table I), with the weaker mechanical interfacial relaxation (Fig. 4), and with the lower σ_{dc} values in the rubbery state (Fig. 6), all of which indicate more robust interfaces compared to the respective composites with noncovalently-bonded fillers.

The combined performance across all above properties, shows that chemically bonding the two nanofillers together allows for synergistically exploiting the properties of the inorganic fillers, while minimizing the formation of weak polymer/BT interfaces, which may deteriorate the composites' dielectric properties. A significant improvement in the dielectric breakdown strength values was also found for these composites and is discussed below.

2. Dielectric breakdown

The characteristic electric breakdown strength of the composites is analyzed within the frame of Weibull statistics.[46,47] The Weibull model is the most widely used method to describe the statistical behavior of electrical or mechanical strength properties of many materials, including composites, and is given by:

$$P(\alpha,\beta,E_{BD}) = 1 - \exp[-(E_{BD}/\alpha_w)^{\beta_w}], \quad (3)$$

where *P* represents the cumulative probability function of the breakdown distribution; the Weibull modulus β_w is a material parameter that characterizes the scattering in the measured values of the breakdown strength, E_{BD}; and the scale parameter, α_w, otherwise known as estimator value in E_{BD}, is the value of E_{BD} at which the cumulative probability is 0.6321 $(1-e^{-1})$.

Figure 8 shows the Weibull plots for the unfilled epoxy and the composite with 5 wt % in BT/oMMT. The parameters β_w and α_w, essential for the complete characterization of the material, were calculated from the slope and the ordinate at the origin. The Weibull modulus β_w quantifies the scattering in the experimental data and a higher value of β_w represents less scattering. The calculated values of β_w are found to be 16.61 for the 5 wt % in BT/oMMT composite, and 8.29 for the unfilled epoxy. Also, the characteristic breakdown strength (α_w parameter) for the same composite is 3.6 MV/cm, which is similar with that of the unfilled epoxy (3.8 MV/cm). In addition, the 10 wt % BT/oMMT composite shows a similar breakdown strength, α_w, whereas the characteristic breakdown strength decreases for the 15 and 20 wt % BT/oMMT composites. This is in excellent agreement with the trends observed in the glass transition temperature, in the conductivity, and in the σ_{dc} activation energies, as discussed previously. Thus any detrimental effects in the performance of the epoxy composites under high electric fields, when adding both high permittivity BT fillers and high aspect ratio oMMT fillers, are significantly reduced in the present systems, when the two fillers are covalently bonded to each other and adopt the configuration shown in Figs. 1(c)–1(f). The achieved combination of large high-field permittivity, low losses, and large dielectric breakdown strengths can be advantageous in the development of compact energy storage materials.

IV. CONCLUSIONS

BT and MMT nanoparticles were covalently bonded in solution, forming hybrid nanofillers with BT cores bearing chemically attached oMMT layers. These hybrid nanoparticulates were subsequently dispersed in epoxy resin, yielding nanocomposites that exhibited good dispersions even at high filler loadings. This approach led to a unique spatial configuration of the nanofillers, that consists of BT spherical nanoparticles surrounded by covalently-bonded layered MMT platelets. This filler configuration, in conjunction with a reactive-oMMT nanofillers that could crosslink with the epoxides, evidently resulted in stronger interfaces with the epoxy matrix, compared to the respective single-filler composites (i.e., epoxy composites with either BT or nonreactive-oMMT fillers at similar concentrations). Specifically, the thermodynamic investigation of the glass transition process showed an increase in the glass transition temperature and indicated the formation of immobilized (tightly bound) polymer at the filler interfaces. Dynamic mechanical analysis further showed a significant improvement of the storage modulus at low temperatures, and detected a relaxation which varies with the filler loading and seems to arise from the interfaces; above the T_g DMA showed an increase in the plateau modulus.

From the dielectric performance viewpoint, the unique filler structure, resulted from the covalent bonding of BT and oMMT, was found to synergistically combine the good properties of the two individual inorganic phases, i.e., the high permittivity of the BT and the good interfacial properties of the reactive MMT. The resulting nanocomposites demonstrated good electrical properties under low and high electric

fields. The dc conductivity above the T_g and at low filler content (5 wt %) was found to be lower than the value for the unfilled epoxy, whereas the same composite under high electric fields exhibited minimal high-field losses and higher permittivity than the unfilled epoxy. These concurrent improvement in permittivity and the low losses, combined with the formation of robust interfaces, resulted also to a better distribution of the dielectric breakdown strength values, compared to the unfilled epoxy. The combination of enhancements in thermomechanical and electrical properties in these systems can be utilized in the design of high performance materials for energy storage and electrical insulation applications.

ACKNOWLEDGMENTS

This work was supported by the Office of Naval Research (Grant No. MURI-00014-05-1-0541). G.P. and E.M. acknowledge additional financial support by the National Science Foundation (NSF) (Grant No. DMR-0602877).

[1] *Polymeric Nanocomposite Dielectrics* edited by J. K. Nelson (Springer, New York, 2009).
[2] Y. Cao, P. C. Irwin, and K. Younsi, IEEE Trans. Dielectr. Electr. Insul. **11**, 797 (2004).
[3] G. C. Montanari, D. Fabiani, F. Palmieri, D. Kaempfer, R. Thomann, and R. Mülhaupt, IEEE Trans. Dielectr. Electr. Insul. **11**, 754 (2004).
[4] E. Tuncer, I. Sauers, D. R. James, A. R. Ellis, M. P. Paranthaman, T. Aytug, S. Sathyamurthy, K. L. More, J. Li, and A. Goyal, Nanotechnology **18**, 025703 (2007).
[5] E. Tuncer, I. Sauers, D. R. James, A. R. Ellis, M. P. Paranthaman, A. Goyal, and K. L. More, Nanotechnology **18**, 325704 (2007).
[6] G. Polizos, E. Tuncer, I. Sauers, and K. L. More, Appl. Phys. Lett. **96**, 152903 (2010).
[7] M. Alexandre and P. Dubois, Mater. Sci. Eng. R. **28**, 1 (2000).
[8] T. Lan, P. D. Kaviratna, and T. J. Pinnavaia, Chem. Mater. **7**, 2144 (1995).
[9] E. P. Giannelis, R. Krishnamoorti, and E. Manias, Adv. Polym. Sci. **138**, 107 (1999).
[10] P. B. Messersmith and E. P. Giannelis, J. Polym. Sci. A Polym. Chem. **33**, 1047 (1995).
[11] E. P. Giannelis, Adv. Mater. **8**, 29 (1996).
[12] J. Choi, A. F. Yee, and R. M. Laine, Macromolecules **36**, 5666 (2003).
[13] J. Zhang, E. Manias, and C. A. Wilkie, J. Nanosci. Nanotechnol. **8**, 1597 (2008).
[14] E. Manias, A. Touny, L. Wu, K. Strawhecker, B. Lu, and T. C. Chung, Chem. Mater. **13**, 3516 (2001).
[15] E. Manias, J. Zhang, J. Y. Huh, K. Manokruang, P. Songtipya, and M. M. Jimenez-Gasco Macromol. Rapid Commun. **30**, 17 (2009); J. Zhang, E. Manias, G. Polizos, J. Y. Huh, A. Ophir, P. Songtipya, and M. M. Jimenez-Gasco, J. Adhes. Sci. Technol. **23**, 709 (2009).
[16] E. Manias, Nature Mater. **6**, 9 (2007).
[17] M. Roy, J. K. Nelson, R. K. MacCrone, L. S. Schadler, C. W. Reed, R. Keefe, and W. Zenger, IEEE Trans. Dielectr. Electr. Insul. **12**, 629 (2005).
[18] D. Ma, T. A. Hugener, R. W. Siegel, A. Christerson, E. Martensson, C. Önneby, and L. S. Schadler, Nanotechnology **16**, 724 (2005).
[19] V. Tomer, G. Polizos, E. Manias, and C. A. Randall, J. Appl. Phys. **108**, 074116 (2010).
[20] Z. Lu, G. Polizos, D. D. Macdonald, and E. Manias, J. Electrochem. Soc. **155**, B163 (2008).
[21] V. Tomer, C. A. Randall, G. Polizos, J. Kostelnick, and E. Manias, J. Appl. Phys. **103**, 034115 (2008).
[22] Z. Lu, E. Manias, D. D. Macdonald, and M. Lanagan, J. Phys. Chem. A **113**, 12207 (2009).
[23] V. Tomer and C. A. Randall, J. Appl. Phys. **104**, 074106 (2008).
[24] D. P. Agoris, I. Vitellas, O. S. Gefle, S. M. Lebedev, and Y. P. Pokholkov, J. Phys. D: Appl. Phys. **34**, 3485 (2001).
[25] A calculation of the required stoichiometric ratio of the curing agent for the composites was not performed. Such a calculation necessitates correct enumeration of the weight fraction of the amine groups present in the filler, which participate in the crosslinking process; however, since the TETA groups are tethered on the MMT surfaces, their effective concentration depends strongly on the dispersion of oMMT (the extent of dispersion is not known a priori and neither can it be exactly dictated by formulation or processing).
[26] H. Koerner, D. Misra, A. Tan, L. Drummy, P. Mirau, and R. Vaia, Polymer **47**, 3426 (2006).
[27] G. Polizos, E. Tuncer, I. Sauers, and K. L. More, "Physical properties of epoxy resin/titanium dioxide nanocomposites," Polym. Eng. Sci. (to be published).
[28] S. Ramesh, B. A. Shutzberg, C. Huang, J. Gao, and E. P. Giannelis, IEEE Trans. Adv. Packag. **26**, 17 (2003).
[29] O. Becker, R. Varley, and G. Simon, Polymer **43**, 4365 (2002).
[30] F. Hussain, J. Chen, and M. Hojjati, Mater. Sci. Eng., A **445–446**, 467 (2007).
[31] E. Manias, V. Kuppa, D. B. Zax, and D. K. Yang, Colloids Surf., A **187–188**, 509 (2001).
[32] B. Wunderlich, Prog. Polym. Sci. **28**, 383 (2003).
[33] F. D. Blum, E. N. Young, G. Smith, and O. C. Sitton, Langmuir **22**, 4741 (2006).
[34] V. Kuppa, T. M. D. Foley, and E. Manias, Eur. Phys. J. E **12**, 159 (2003).
[35] C. Chen and D. Curliss, Nanotechnology **14**, 643 (2003).
[36] J. Chandradass and D. S. Bae, Mater. Manuf. Processes **23**, 116 (2008).
[37] E. Manias and V. Kuppa, Eur. Phys. J. E **8**, 193 (2002).
[38] W. H. Awad, G. Beyer, D. Benderly, W. L. Ijdo, P. Songtipya, M. M. Jimenez-Gasco, E. Manias, and C. A. Wilkie, Polymer **50**, 1857 (2009).
[39] L. Xu, H. Nakajima, E. Manias, and R. Krishnamoorti, Macromolecules **42**, 3795 (2009).
[40] S. Havriliak and S. Negami, Polymer **8**, 161 (1967).
[41] *Broadband Dielectric Spectroscopy*, edited by F. Kremer and A. Schönhals (Springer-Verlag, Berlin, 2002).
[42] E. Manias, G. Hadziioannou, and G. ten Brinke, J. Chem. Phys. **101**, 1721 (1994).
[43] G. Polizos, V. V. Shilov, and P. Pissis, Solid State Ionics **145**, 93 (2001).
[44] C. J. Dias and D. K. Das Gupta, IEEE Trans. Dielectr. Electr. Insul. **3**, 706 (1996).
[45] L. E. Cross, Mater. Chem. Phys. **43**, 108 (1996).
[46] W. Weibull, ASME J. Appl. Mech. **18**, 293 (1951).
[47] S. M. Rowland, R. M. Hill, and L. A. Dissado, J. Phys. C **19**, 6263 (1986).